J Mater Sci (2011) 46:3200–3206
DOI 10.1007/s10853-010-5204-y

Structural and optical characterization of Ni-doped CdS quantum dots

M. Thambidurai · N. Muthukumarasamy · S. Agilan · N. Sabari Arul · N. Murugan · R. Balasundaraprabhu

Received: 28 October 2010 / Accepted: 17 December 2010 / Published online: 29 December 2010

Abstract Ni-doped CdS quantum dots have been prepared by chemical precipitation technique. The X-diffraction results indicated that the particle size of Ni-doped CdS nanoparticles is smaller than that of undoped CdS and no secondary phase was observed. The average grain size of the nanoparticles is found to lie in the range of 2.7–4 nm. The compositional analysis results show that Cd, Ni, and S are present in the samples. HRTEM studies reveal that the average particle size of undoped and Ni-doped CdS quantum dots is 2 and 3 nm, respectively. Raman spectra shows that 1LO, 2LO, and 3LO peaks of the Ni-doped CdS samples are slightly red shifted when compared to that of undoped CdS. The absorption edge of Ni-doped CdS nanoparticles is found to shift towards the higher-wavelength (red shift) side when compared to that of undoped CdS and the band gap is observed to lie in the range of 3.79–3.95 eV. This band gap is higher than that of the bulk CdS and is due to quantum confinement effect present in CdS nanoparticles.

M. Thambidurai (✉) · N. Muthukumarasamy · S. Agilan
Department of Physics, Coimbatore Institute of Technology, Coimbatore, India
e-mail: phy_thambi@rediffmail.com

N. Sabari Arul
Department of Nanoscience and Technology, Bharathiar University, Coimbatore, India

N. Murugan
Department of Mechanical Engineering, Coimbatore Institute of Technology, Coimbatore, India

R. Balasundaraprabhu
Department of Physics, PSG College of Technology, Coimbatore, India

Introduction

Nanomaterials exhibit electrical and optical properties which depends sensitively on the size of the nanocrystals and the properties are of both fundamental and technological interest. Binary chalcogenide nanocrystalline semiconductors such as PbS, ZnS, ZnSe, CdS, and CdSe have attracted considerable attention in recent years due to their unique properties, which arise due to size quantization [1–5]. Among them, CdS is one of the most important group II–VI semiconductor, having a typical band gap of 2.42 eV at room temperature and is used in solar cells, biological labels, waveguides, and photoconductors [6–10]. It is particularly interesting to see what happens when the size of the nanoparticle becomes smaller than or comparable to the radius of the orbit of the electron–hole pair (Bohr exciton radius). There are two situations, called the weak confinement and the strong confinement regimes. In the weak regime the particle radius is larger than the radius of the electron–hole pair, but the range of motion of the exciton is limited, which causes a blue shift in the absorption spectrum. When the radius of the particle is smaller than the orbital radius of electron–hole pair, the motion of electron and hole become independent and the exciton does not exist. The hole and the electron have their own set of energy levels. Here also there is a blue shift [11]. The Bohr radius of the exciton is 3 nm for CdS and the quantum confinement occurs when the size of the crystallite is around 2–6 nm and below [12]. This confinement induces discrete electronic states in the valence and conduction band of the quantum dots compared to the continuous state of energy in the bulk material. If the crystallite size is below the exciton Bohr radius of the semiconductor, strong quantum confinement occurs. The confinement effect appears as a shift in the absorption

spectra (blue shift) and the absorption edge is shifted to lower wavelengths, which is due to the change in the band gap. The absorption shift and spectral features can be used to measure the particle size. For CdS, the quantum confinement effect can be observed when the particle size is less than 6 nm. CdS has a bulk absorption edge at 512 nm and this can decrease to 97 nm for very small CdS particles due to the quantum confinement effect [13].

Nanocrystalline CdS has been prepared by different workers using various techniques such as pulsed laser deposition, chemical bath deposition, spray pyrolysis, successive ionic layer adsorption and reaction, screen printing and sol–gel spin coating method [14–19] with controlled particle size distribution. Doping is important for semiconductors, which plays a critical role in tuning their optical and electrical properties for the potential application in solar cells [20] and photocatalysis [21]. Doping of CdS nanostructures with other materials has attracted immense attention in recent years. A new peak appears in the photoluminescence spectra of Mn-doped CdS nanocrystal due to Mn *d–d* transition [22]. Fe-doped CdS has been prepared by Godbole et al. [23] using spray pyrolysis technique and they have reported that Fe acts as killer centers for photoconductivity. Ma et al. [24] have reported that Raman peaks of the CdS nanoparticles get enhanced with increasing Ag^{+} concentration. But not much work has been reported on Ni-doped CdS. In this article, we report about the preparation, structural, and optical properties of undoped and Ni-doped CdS quantum dots.

Experimental

In the present study, Ni-doped CdS quantum dots have been synthesized through chemical precipitation technique. Aqueous solution of cadmium nitrate (Cd $(NO_3)_2{\cdot}4H_2O$) and required amount of nickel nitrate (Ni $(NO_3)_2{\cdot}6H_2O$) were stirred for 1 h at room temperature. Aqueous solution of sodium sulfide (Na_2S) was added drop wise to (cadmium nitrate + nickel nitrate) the solution and was stirred for 2 h. A precipitate with yellowish orange color was formed soon after the addition of the Na_2S. The nanoparticles were initially purified by precipitating the particles with excess double distilled water and the solution obtained was centrifuged at 4,000 rpm for 10 min. The sample was obtained as precipitate and after that the sample was dried at 80 °C for 4 h.

X-ray diffraction studies have been carried out using PANalytical X-ray diffractometer, surface morphology of the samples has been studied using JEM JEOL-6500 Field emission scanning electron microscope (FESEM), the composition of the prepared samples has been studied by energy dispersive X-ray analysis (EDAX, Thermo-Noran system Six) and high resolution transmission electron microscope (HRTEM) images of the prepared CdS and Ni-doped CdS have been recorded using a Philips TECNAI F20 microscope. Raman spectra of the samples have been recorded using JOBIN–YVON OF ir-550 spectrometer. The optical properties have been studied using the absorbance spectrum recorded using spectrophotometer (JASCO-V-570).

Results and discussion

The structural characterization of the nanoparticles has been carried out by X-ray diffraction technique using CuKα radiation. X-ray diffraction patterns of CdS and Ni-doped CdS nanoparticles are shown in Fig. 1. The diffraction pattern exhibits broad peaks revealing that the prepared particles are of very small crystallite size. All the peaks in the diffraction pattern is found to be characteristic of CdS, suggesting that incorporation of Ni in the sample does not introduce appreciable change in the crystal structure of CdS. The diffraction peaks at 2θ (degree) values of 26.60°, 43.92° and 51.93° of CdS correspond to the (002), (110) and (112) planes of hexagonal CdS. The lattice constants have been found to be $a = 4.116$ Å and $c = 6.694$ Å which is in agreement with the standard JCPDS data (JCPDS card no. 02-0549). Table 1 shows the structural parameters of the undoped and Ni-doped CdS nanoparticles. It is observed that the lattice constant "*a*" and "*c*" decreases with increase in Ni concentration. It is also seen that the Bragg angle (2θ) of the intense (002) reflection exhibits a slight shift towards higher 2θ values with increase in Ni concentration. The absence of the

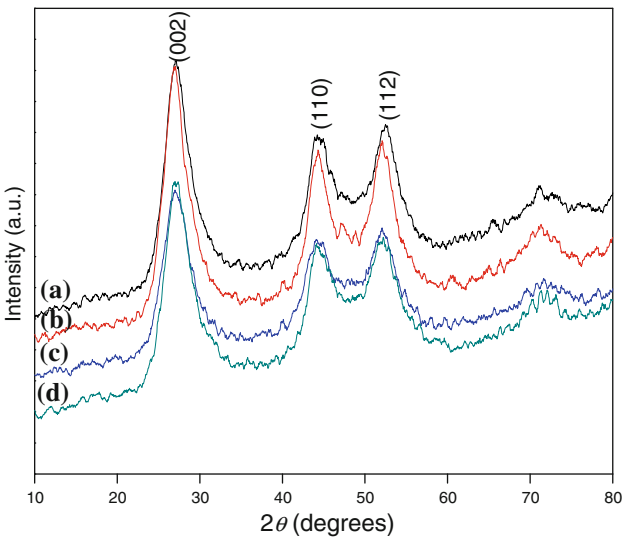

Fig. 1 X-ray diffraction pattern of **a** CdS, **b** 1.76% Ni, **c** 3.23% Ni, and **d** 4.96% Ni-doped CdS

Table 1 Structural parameters of CdS and Ni-doped CdS nanoparticles

Material	$2\theta_{(002)}$	d (Å)	Calculated values		Grain size (nm)
			a (Å)	c (Å)	
CdS	26.60	3.347	4.116	6.694	2.7
1.76% Ni	26.68	3.336	4.110	6.672	3.1
3.23% Ni	26.78	3.324	4.102	6.648	3.6
4.96% Ni	26.91	3.309	4.088	6.618	4.0

diffraction peaks of NiS phase in the pattern implies that Ni substitutes for Cd in the prepared Ni-doped CdS. No other impurity phase is observed, which indicates that the Ni ion successfully occupies the lattice site rather than the interstitial ones. With increase of the content of Ni the lattice parameters is observed to decrease and this is due to the fact that the radius of the Ni ion is smaller than that of Cd^{2+}. The size of CdS nanoparticles has been calculated using Scherrer's equation [25]:

$$D = \frac{K\lambda}{\beta \cos\theta} \quad (1)$$

where, D is the grain size, K a constant taken to be 0.94, λ the wavelength of the X-ray radiation, β the full width at half maximum, and θ is the angle of diffraction. The particle size has been calculated and is found to be 2.7, 3.1, 3.6, and 4.0 ($\pm$0.1) nm for undoped CdS, 1.76% Ni, 3.23% Ni, and 4.96% Ni-doped CdS, respectively.

The surface morphology of the samples has been studied using field emission scanning electron microscope (FESEM). Figure 2 shows the FESEM images of CdS and Ni-doped CdS samples. FESEM images suggest that the samples have uniform grain distribution with well connected grains. Figure 3a–d shows the energy dispersive X-ray analysis (EDAX) of the undoped and Ni-doped CdS. The chemical constituents present in the sample according to the EDAX analysis are Cd = 49.23% and S = 50.77% for undoped CdS, Cd = 49.04%, S = 49.20% for 1.76% Ni, Cd = 47.67%, S = 49.10% for 3.23% Ni and Cd = 46.24%, S = 48.80% for 4.96% Ni-doped CdS.

The size of the undoped and Ni-doped CdS nanoparticles has been studied using high resolution transmission electron microscope (HRTEM). The HRTEM images of CdS and Ni-doped CdS are shown in Fig. 4. There are no visible single particles in the HRTEM images (Fig. 4a, c) and it is observed that all the particles have agglomerated. The interplanar lattice spacing of the planes seen in the micrograph of undoped CdS is found to be 3.35 Å and that corresponds to the (002) plane of hexagonal CdS. Ni-doped CdS nanoparticles have a slightly less lattice spacing of 3.32 Å and this is due to the small ionic radius of Ni^{2+}

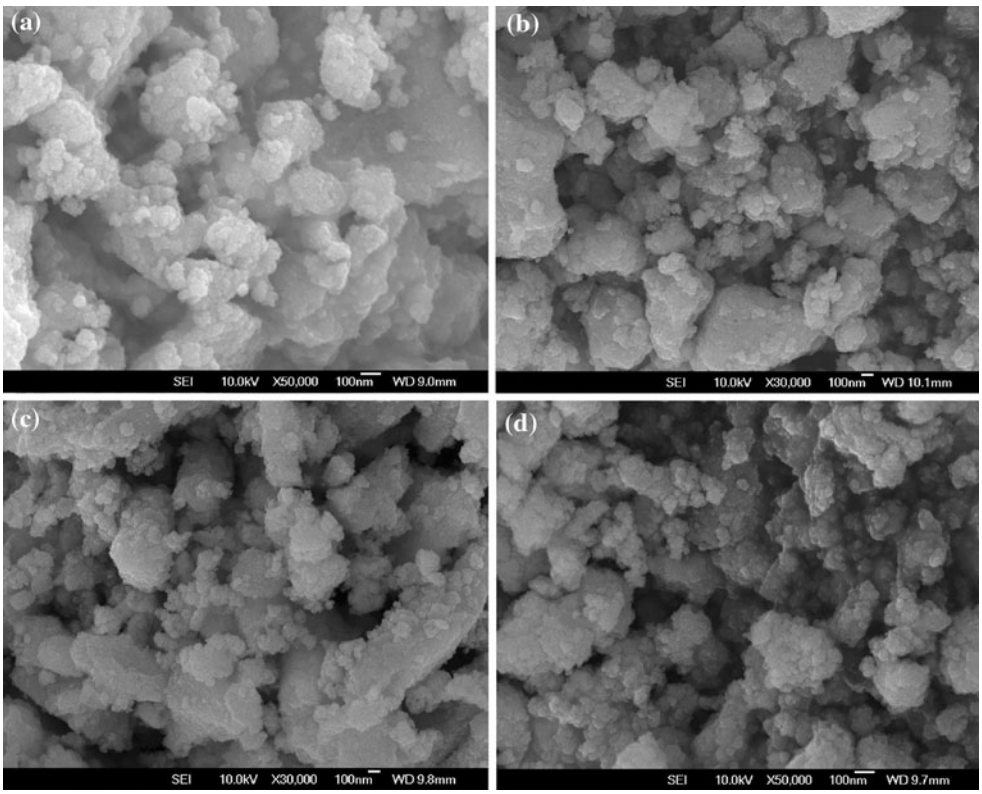

Fig. 2 FESEM images of **a** CdS and Ni-doped CdS, **b** 1.76% Ni, **c** 3.23% Ni, and **d** 4.96% Ni-doped CdS quantum dots

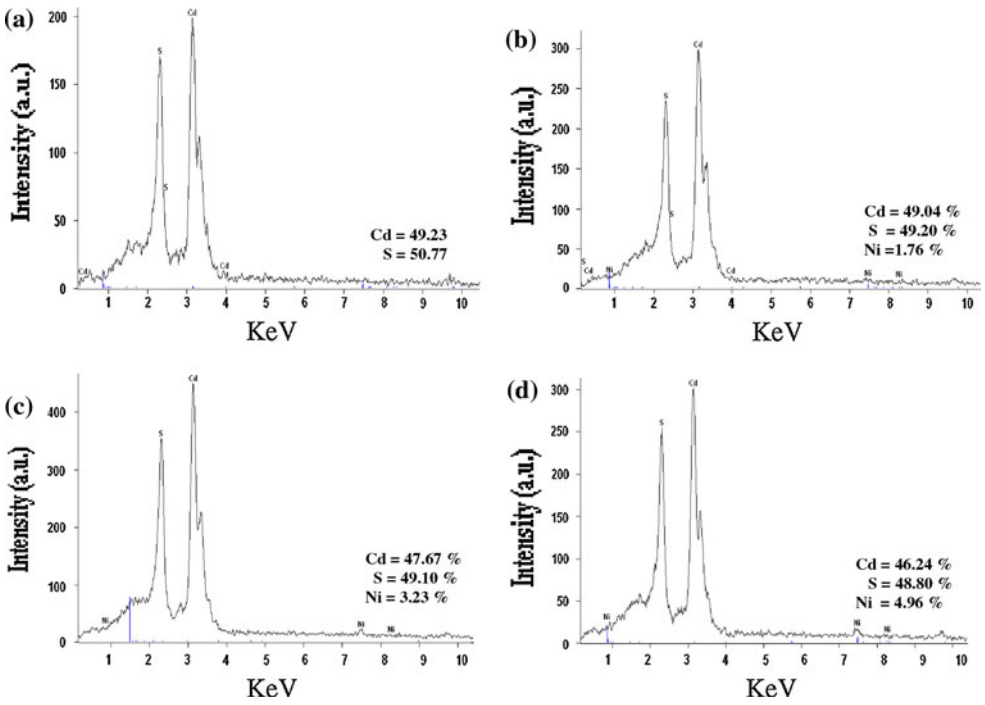

Fig. 3 EDAX pattern of CdS and Ni-doped CdS

when compared to that of Cd^{2+} ($r_{Ni}^{2+} = 0.62$ Å, $r_{Cd}^{2+} = 0.96$ Å). The *d* spacing values calculated from these images are in close agreement with the values obtained from X-ray diffraction studies. The HRTEM image of the undoped and Ni-doped CdS nanoparticles also shows that the particle size lies in the range of about ~2–3 nm.

Raman spectra of CdS and Ni-doped CdS nanoparticles recorded in the 1LO, 2LO, and 3LO mode region are shown in Fig. 5. Raman spectra (Fig. 5) of CdS show three main peaks at 300, 601, and 900 cm^{-1}, respectively, and these Raman peaks of CdS are in agreement with the reported values [26–28]. Compared with these Raman modes (300, 601, and 900 cm^{-1}) of CdS nanoparticles, the Raman modes of Ni-doped CdS nanoparticles are slightly red shifted and are observed at 293, 593, and 893 cm^{-1}, respectively.

Optical absorption spectra has also been used to determine the size of the nanoparticles. Optical absorption spectra of CdS and Ni-doped CdS quantum dots are shown in Fig. 6. The absorption edge of the CdS samples exhibit a strong blue shift when compared to the value of bulk CdS (512 nm) and it clearly indicates the formation of CdS nanoparticles. The absorption edge is blue shifted when the size of semiconductor nanoparticles decreases [29]. The absorption edge of the undoped and Ni-doped CdS spectra shown in Fig. 6 exhibits a large blue shift, with the absorption edge lying in the range of 330–390 nm. The absorption edge of Ni-doped CdS shifts towards longer wavelength with increasing Ni concentration when compared to undoped CdS. This indicates that there is a decrease in energy band gap of CdS on Ni doping. According to Yao et al. [30] CdS nanoparticles with absorption peaks at 505, 504, 494, and 491 nm correspond to particle size of 6.4, 6.3, 5.5, and 5.3 nm, respectively.

The fundamental absorption, which corresponds to the electron excitation from the valence band to the conduction band, can be used to determine the nature and value of the optical band gap. The relation between the absorption coefficient (α) and the incident photon energy ($h\upsilon$) can be written as

$$(\alpha h\upsilon) = A\left(h\upsilon - E_g\right)^n \quad (2)$$

where *A* is a constant, E_g the band gap of material, υ the frequency of the incident radiation, *h* the Planck's constant and the exponent *n* is 0.5 for direct allowed transitions. The optical band gap of the undoped and Ni-doped CdS nanoparticles have been calculated using Eq. 2. The direct band gap values have been obtained from the linear portion of $(\alpha h\upsilon)^2$ vs. $h\upsilon$ plot shown in Fig. 7 and the band gap values are given in Table 2. The band gap of CdS should decrease with the increase in Ni concentration because the band gap of CdS is higher than that of NiS [31]. From Table 2 it is clearly seen that within the quantum confinement regime band gap becomes a function of the particle size and decreases with increasing particle size, however, only a small change in band gap has been observed due to incorporation of Ni in CdS. The observed direct band gap is much higher than that of the bulk value of CdS (2.42 eV), because of the quantum confinement effect present in the CdS nanocrystals. Gemma has

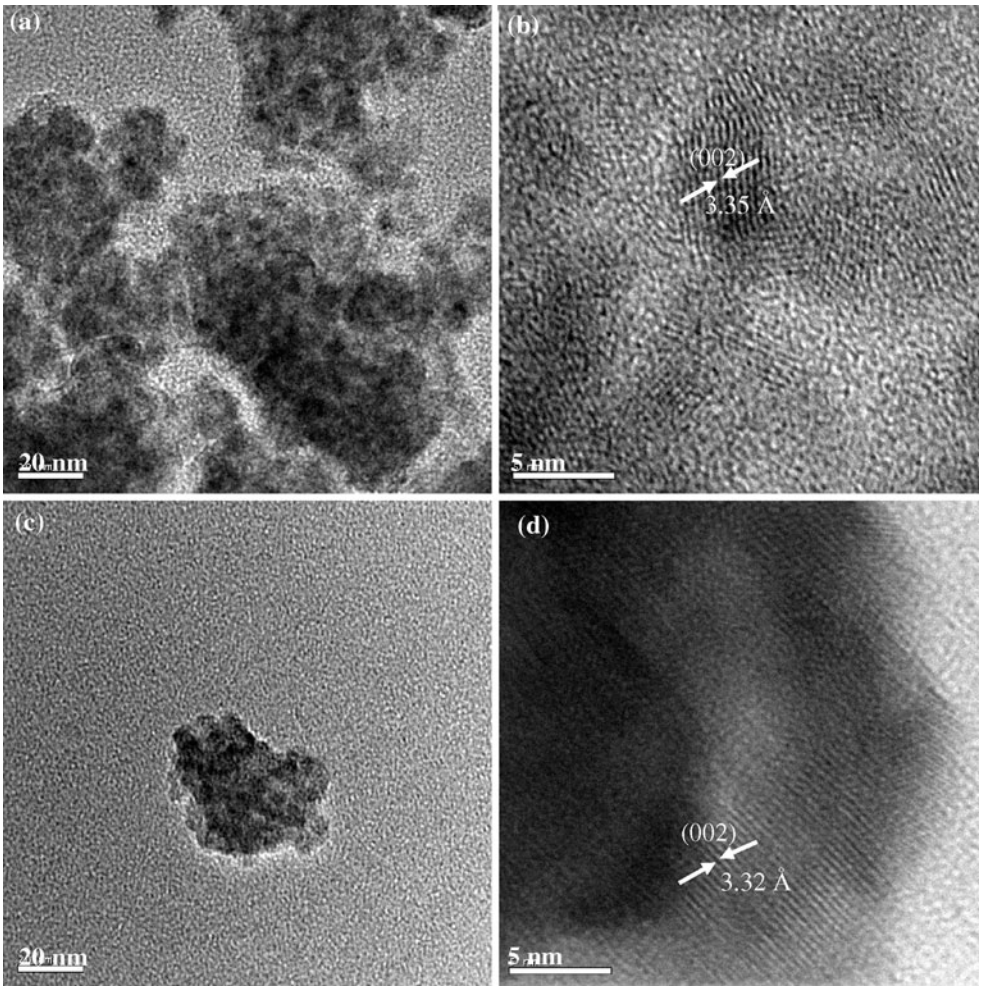

Fig. 4 HRTEM images of **a**, **b** CdS and **c**, **d** 3.23% Ni-doped CdS

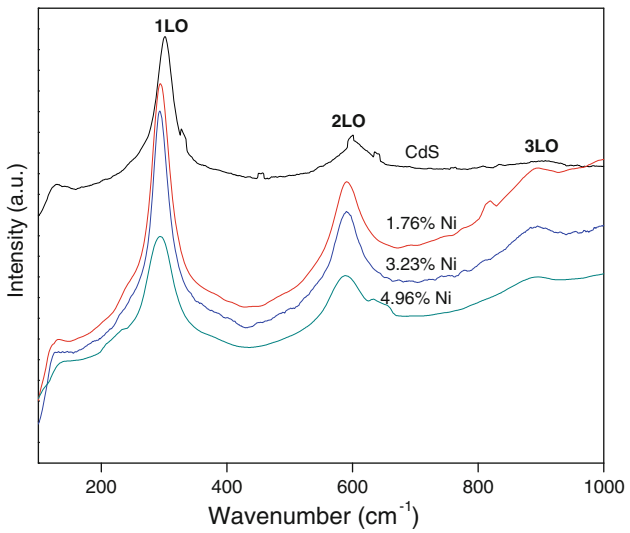

Fig. 5 Raman spectra of CdS and Ni-doped CdS

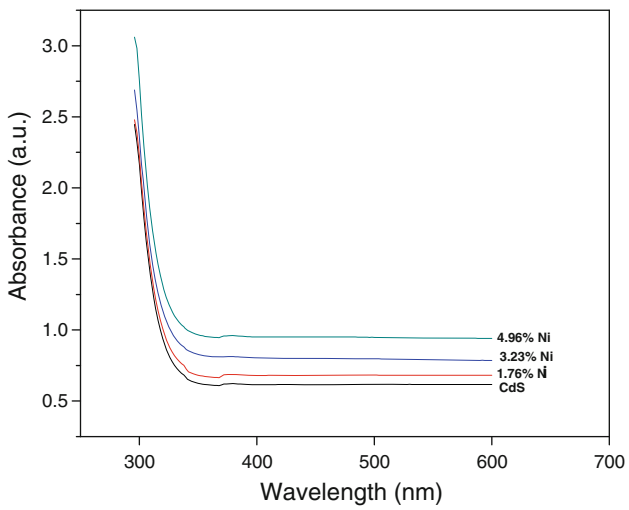

Fig. 6 Optical absorption spectra of CdS and Ni-doped CdS

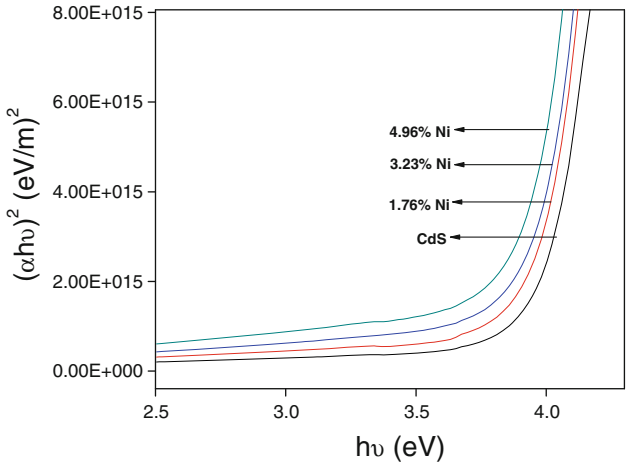

Fig. 7 Plot of $(\alpha h\upsilon)^2$ vs. $h\upsilon$ of CdS and Ni-doped CdS

Table 2 Particle size obtained from the blue shift of optical band gap (E_g) for CdS and Ni-doped CdS

Material	Band gap (*eV*)	Particle size (nm)
CdS	3.95	2.2
1.76% Ni	3.89	2.4
3.23% Ni	3.84	2.6
4.96% Ni	3.79	2.8

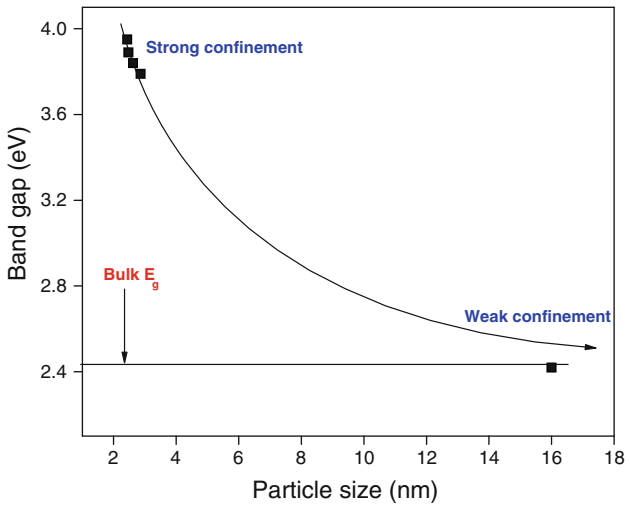

Fig. 8 Variation of band gap of CdS and Ni-doped CdS with particle size showing strong and weak confinement region

reported that substitution of only transition metal impurity in CdS, ZnS, ZnO, GaP changes the band gap values [32]. Similar results of band gap variation have also been reported in Mn-doped CdS films [33], Fe-doped CdS bulk crystals [34], and Ga-doped CdS [35]. The nanocrystalline CdS particles should have a wider band gap than the bulk material because of the quantum confinement of the electron–hole pair. The larger energy difference causes a shift in the visible absorption spectrum of CdS. The blue shift in the band gap of nanoparticles due to quantum confinement is of the quantitative form [36]:

$$E_g^{\text{nano}} = E_g^{\text{bulk}} + \frac{h^2\pi^2}{2\mu R^2} - \frac{1.8e^2}{\varepsilon R} \quad (3)$$

where E_g^{nano} and E_g^{bulk} are the band gap values of the nanoparticles and the bulk material, respectively, $\mu = m_e \cdot m_h/(m_e + m_h)$ is the reduced mass and m_e and m_h are the effective masses of electron (0.21 m for CdS) in the conduction band and holes (0.80 m for CdS) in the valence band, respectively, e is the electron charge, ε is the relative permittivity of the semiconductor, R is the radius of the particle and the second term is the columbic term and is generally neglected. The particle size has been calculated using the blue shift of the optical band gap caused by quantum confinement and the particle size is found to be in the range of 2.2–2.8 nm. Quantum confinement of both electrons and holes in all three dimensions leads to an increase in the effective band gap of the material with decreasing particle size. It is clearly observed from Fig. 8 that strong confinement is present in the CdS and Ni-doped CdS particles. As the particle size obtained from X-ray diffraction, HRTEM and optical band gap studies is smaller than the Bohr excitation radius of 3 nm for CdS, the strong confinement effect can be assumed to be present in the prepared CdS and Ni-doped CdS quantum dots.

Conclusion

Ni-doped CdS quantum dots have been prepared by chemical precipitation technique. X-ray diffraction analysis reveals that CdS and Ni-doped CdS quantum dots exhibit hexagonal structure and the average particle size is found to lie in the range of 2.7–4.0 nm. The lattice constants of CdS nanoparticles decrease slightly with Ni doping in CdS. The HRTEM image shows the formation of CdS and Ni-doped CdS quantum dots with an average particle size of 2–3 nm. The band gap of CdS and Ni-doped CdS nanoparticles is observed to decrease with increase in particle size due to quantum size effect and the particle size is in range of 2.2–2.8 nm.

Acknowledgement The authors thank the University Grants Commission, India for providing financial support.

References

1. Navaneethan M, Nisha KD, Ponnusamy S, Muthamizhchelvan C (2009) Mater Chem Phys 117:443
2. Unn C, Philip D, Gopchandran KG (2009) Optic Mater 32:169

3. Andrade JJ, Brasil AG Jr, Farias PMA, Fontes A, Santos BS (2009) Microelectron J 40:641
4. Thambidurai M, Murugan N, Muthukumarasamy N, Vasantha S, Balasundaraprabhu R, Agilan S (2009) Chalcogenide Lett 6:171
5. Gao Y, Zhang Q, Gao Q, Tian Y, Zhou W, Zheng L, Zhang S (2009) Mater Chem Phys 115:724
6. Romeo N, Bosio A, Romeo A (2010) Sol Energy Mater Sol Cells 94:2
7. Bruchez M Jr, Moronne M, Gin P, Weiss S, Alivisatos AP (1998) Science 281:2013
8. Agarwal R, Barrelet CJ, Lieber CM (2005) Nano Lett 5:917
9. Gao T, Li QH, Wang TH (2005) Appl Phys Lett 86:173105
10. Lee W, Min SK, Dhas V, Ogale SB, Han SH (2009) Electrochem Commun 11:103
11. Poole CP Jr, Owens FJ (2003) Introduction of nanotechnology. Wiley, New Jersey
12. Yadav RS, Mishra P, Mishra R, Kumar M, Pandey AC (2010) Ultrason Sonochem 17:116
13. Reda SM (2008) Acta Mater 56:259
14. Tong XL, Jiang DS, Hu WB, Liu ZM, Luo MZ (2006) Appl Phys A 84:143
15. Pradhan B, Sharma AK, Ray AK (2007) J Cryst Growth 304:388
16. Raji P, Sanjeeviraja C, Ramachandran K (2005) Bull Mater Sci 28:233
17. Kalandaragh YA, Muradov MB, Mammedov RK, Kaodayari A (2007) J Cryst Growth 305:175
18. Patidar D, Sharma R, Jani N, Sharma TP, Saxena NS (2006) Bull Mater Sci 29:21
19. Luccio TD, Piscopiello E, Laera AM, Antisari MV (2007) Mater Sci Eng C 27:1372
20. Lee J-H, Yi J-S, Yang K-J, Park J-H, Oh R-D (2003) Thin Solid Films 431–432:344
21. Zyoud AH, Zaatar N, Saadeddin I, Ali C, Park D, Campet G, Hilal HS (2010) J Hazard Mater 173:318
22. Nag A, Sapra S, Sen Gupta S, Prakash A, Ghangrekar A, Periasamy N, Sarma DD (2008) Bull Mater Sci 31(3):561
23. Badera N, Godbole B, Srivastava SB, Vishwakarma PN, Sharath Chandra LS, Jain D, Gangrade M, Shripathi T, Sathe VG, Ganesan V (2008) Appl Surface Sci 254:7042
24. Ma J, Tai G, Guo W (2010) Ultrasonic Sonochem 17:534
25. Soni H, Chawda M, Bodas D (2009) Mater Lett 63:767
26. Phuruangrat A, Thongtem T, Thongtem S (2009) Mater Lett 63: 1538
27. Thongtem T, Phuruangrat A, Thongtem S (2009) Ceram Int 35:2817
28. Prabhu RR, khaddar MA (2008) Bull Mater Sci 31(3):511
29. Maleki M, Ghamsari MS, Mirdamadi Sh, Ghasemzadeh R (2007) Semiconduct Phys Quantum Electron Optoelectron 10:30
30. Yao L, Xu G, Yang X, Luan Y (2009) Colloids Surface A 333:1
31. Kassim A, Zainal Z, Nagalingam S, Kuang D, Sharafaddin NH, Mai C (2004) Science 31(2):131
32. Gemma N (1984) J Phys C 17:2333
33. Tsai CT, Chen SH, Chu DS (1996) Phys Rev B 54:11555
34. Cho WC, Kuo SS, Chen FR, Twardowski A, Tworzydlo J, Chen YF (1996) Phys Status Solidi B 193:125
35. Khallaf H, Chai G, Lupan O, Chow L, Park S, Schulte A (2009) Appl Surface Sci 255:4129
36. Jhonsi MA, Kathiravan A, Renganathan R (2009) J Mol Struct 921:279